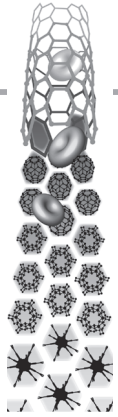

Fluorescent nanothermometers provide controlled plasmonic-mediated intracellular hyperthermia

Aim: This article demonstrates how controlled hyperthermia at the cellular level can be achieved. **Materials & methods**: The method is based on the simultaneous intracellular incorporation of fluorescence nanothermometers (CdSe quantum dots) and metallic nanoheaters (gold nanorods). **Results**: Real-time spectral analysis of the quantum dot emission provides a detailed feedback about the intracellular thermal loading caused by gold nanorods excited at the plasmon frequency. Based on this approach, thermal dosimetry is assessed in such a way that the infrared laser (heating) power required to achieve catastrophic intracellular temperature increments in cancer cells is identified. **Conclusions**: This pure optical method emerges as a new and promising guide for the development of infrared hyperthermia therapies with minimal invasiveness.

Original submitted 6 March 2012; Revised submitted 3 July 2012; Published online 2 December 2012

KEYWORDS: cancer therapy ■ hyperthermia ■ laser thermal effect ■ metallic nanoheaters ■ nanothermometers

Laura Martínez Maestro[1], Patricia Haro-González[2], M Carmen Iglesias-de la Cruz[3], Francisco Sanz-Rodríguez[4], Ángeles Juarranz[4], José García Solé[1] & Daniel Jaque*[1]

[1]Fluorescence Imaging Group, Departamento de Física de Materiales, Facultad de Ciencias, Instituto Nicolás Cabrera, Universidad Autónoma de Madrid, 28049 Madrid, Spain
[2]Departamento de Física Fundamental y Experimental, Electrónica y Sistemas, Universidad de La Laguna, Avd. Astrofísico Francisco Sánchez, s/n, La Laguna, Tenerife, 38206, Spain
[3]Departamento de Fisiología, Facultad de Medicina, Universidad Autónoma de Madrid. C/Arzobispo Morcillo s/n 29029 Madrid, Spain
[4]Departamento de Biología, Facultad de Ciencias, Universidad Autónoma de Madrid, 28049, Spain
**Author for correspondence: daniel.jaque@uam.es*

The fight against cancer is a multifront battle. In addition to the traditional approaches (such as improved chemotherapy drugs, identification of cancer etiologies and the development of novel surgical techniques), new strategies are being proposed motivated by the triumphant entry of nanomedicine into the scene. Nanomedicine is, indeed, at the basis of the recently appearing noninvasive therapeutic strategies, particularly promising in the almost unexplored area of early cancer detection and treatment, even at the cellular level (of the order of 10 µm size) [1–3]. As an example, luminescent nanoparticles (NPs, a few nanometers in size) have already been demonstrated to provide the possibility of high-sensitivity and high-resolution single cancer-cell imaging [4–11]. This fact, indeed, revives the old dream of early-stage cancer diagnostics and treatment. NPs are not only useful for the purpose of cellular imaging, but some of them have also emerged as efficient therapeutic agents [1,12]. Gold NPs of different shapes (including nanocages, nanoshells and nanorods) have been used as biocompatible systems to perform efficient light-induced hyperthermia therapy at both single- and multi-cell levels [13–18]. Of particular interest are those shaped as rods (gold nanorods [GNRs]), as their heating efficiency can be controlled by a proper choice of their dimensions [19], leading to a maximum light-to-heat conversion efficiency. Their operation scheme seems to be quite simple. Once the GNRs are incorporated into the cancer cell, they are externally excited by a laser beam, with a wavelength that should be lying within the biological tissue window (700–900 nm) and, hence, ensuring large tissue penetration depths. Laser radiation promotes the motion of surface charges of the GNRs (i.e., the creation of surface currents). These laser-induced currents cause an efficient intracellular heating, in such a way that intracellular temperature can be elevated up to cytotoxic levels (42–45°C), driving cancer cells to death [13,20]. In addition to the dimensions of the GNRs, the magnitude of this intracellular heating depends on several parameters, some of them easily managed, mainly power and polarization state of infrared laser power [21,22], whereas others are difficult to control, such as the density of GNRs actually incorporated inside the cancer cell. In fact, these uncontrolled parameters represent one of the most important limitations for the achievement of reproducible hyperthermia treatments *in vivo* using GNRs. Such control is essential to regulate the infrared laser-induced intracellular heating and, thus, to avoid an undesirable heat-induced damage in the surrounding healthy tissues. This restriction could be overcome by real-time intracellular temperature reading. The exact measurement of the intracellular temperature increments caused by infrared-excited GNRs would guide the therapy, so that irradiation parameters could be dynamically adjusted. Nevertheless, intracellular thermal reading is not an easy task, being one

Future Medicine part of fsg

of the most challenging objectives that modern biomedicine has.

Up to now, several methods have already been proposed for noninvasive thermometry with a high resolution, including ultrasound thermometry [23], impedance tomography [24], microwave radiometry [25] and MRI [26,27]. Despite the promising results obtained by these techniques, their application for single-cell hyperthermia processes is limited by the maximum spatial resolutions that can be achieved based on them, which are well above the micrometer. Very recently, semiconductor nanocrystals (hereafter, quantum dots [QDs]) have come onto the scene as multifunctional fluorescent nanothermometers (NTs) capable of simultaneously generating intracellular imaging, as well as acting as thermal indicators. Indeed, they have already been used for dynamical thermal monitoring of single cells in the proximity of heat sources or during externally induced thermogenesis processes [28,29]. With respect to previous proposals for noninvasive thermometry, QD-based fluorescent NTs offer outstanding features, such as real sub-micrometric resolutions, high brightness, high biocompatibility, high temperature resolutions (down to 0.2°C) and the possibility of differential targeting by surface functionalization [30,31].

Materials & methods

In this work we show how biocompatible fluorescent CdSe-QDs can be used as NTs for dynamic intracellular temperature measurement during laser-induced hyperthermia of single cells. We demonstrate how the simultaneous incorporation of GNRs (nanoheaters [NHs]) and CdSe-QDs (NTs) opens the possibility of controlled hyperthermia at the cellular level. This novel mechanism of specific and controlled cell death could represent a remarkable step towards new clinically relevant methods for cancer treatment at early stages with minimal invasiveness and, hence, negligible collateral effects.

For the purpose of simultaneous incorporation of NTs and NHs into living cells we prepared a biologically compatible phosphate-buffered saline (PBS) solution containing NTs (CdSe quantum dots) and NHs (GNRs, 41 nm height × 15 nm wide). Both types of NPs are commercial: the CdSe-QDs were provided by Invitrogen Inc. (ref Q21521MP; CA, USA), whereas the GNRs were provided by Nanopartz (UT, USA; bare gold nanorods with surface plasmon resonance at 808 nm). They were properly coated to form well-dispersible solutions in water-like solvents, without having specific functionalization for cell targeting. The CdSe-QDs were coated with amine-derivative poly(ethylene) glycol, which prevents nonspecific interactions and provides a convenient handle for conjugation. The GNRs were 'bare gold nanorods' obtained by 1D surfactant-directed synthesis with appropriate protocols to produce highly monodispersed and well-characterized nanorods. The resultant GNRs were capped with a cetyltrimethylammonium bromide bilayer, in which one polar head faces the gold and the other faces the aqueous solvent. The nonpolar hydrocarbon tails point inward and so face away from the polar solvent. The dimensions (41 × 10 nm) of the GNRs were chosen in order to optimize the photo-thermal treatment efficiency [19]. In fact, recent studies determine that GNRs with these specific dimensions show heating efficiencies (defined as the ratio between absorption and extinction cross sections) as large as 98%. This heating efficiency is higher than that reported for other recognized NHs, such as gold nanocages. Indeed, the heating efficiency of gold nanocages has been found to be close to 70% – that is 30% smaller than that of the GNRs used in this work [17]. In addition, the heating efficiency of GNRs has also been found to be superior to that of nanoshells, varying between 10 and 65% [16]. It is also important to mention that the peak excitation wavelength (surface plasmon resonance wavelength) of the GNRs is close to 808 nm, so that they can be optically excited within the so-called 'biological window' (700–900 nm).

The concentrations of the components in the mixed solution were optimized for sufficiently bright QD-based fluorescence cell imaging (4.8×10^{13} CdSe-QDs per cm^3) and for effective laser-induced hyperthermia (5×10^9 GNRs per cm^3). Figure 1A shows a transmission electron microscopy image of the mixed solution, revealing the random distribution of both NTs and NHs (indicated by arrows). It is important to note that the presence of these two different classes of NPs did not lead to the formation of conglomerates. Furthermore, no evidence of precipitation of any of the two NPs was observed over the weeks. Figure 1B shows the extinction spectrum of the QDs:GNRs:PBS solution which is, indeed, dominated by the characteristic longitudinal surface plasmon resonance of GNRs at 808 nm. On the other hand, the much larger fluorescence efficiency of CdSe-QDs over GNRs [32] makes the fluorescence properties of the mixed solution resemble that of CdSe-QDs. This is illustrated in Figure 1C, which shows the emission spectrum generated by the QDs:GNRs:PBS

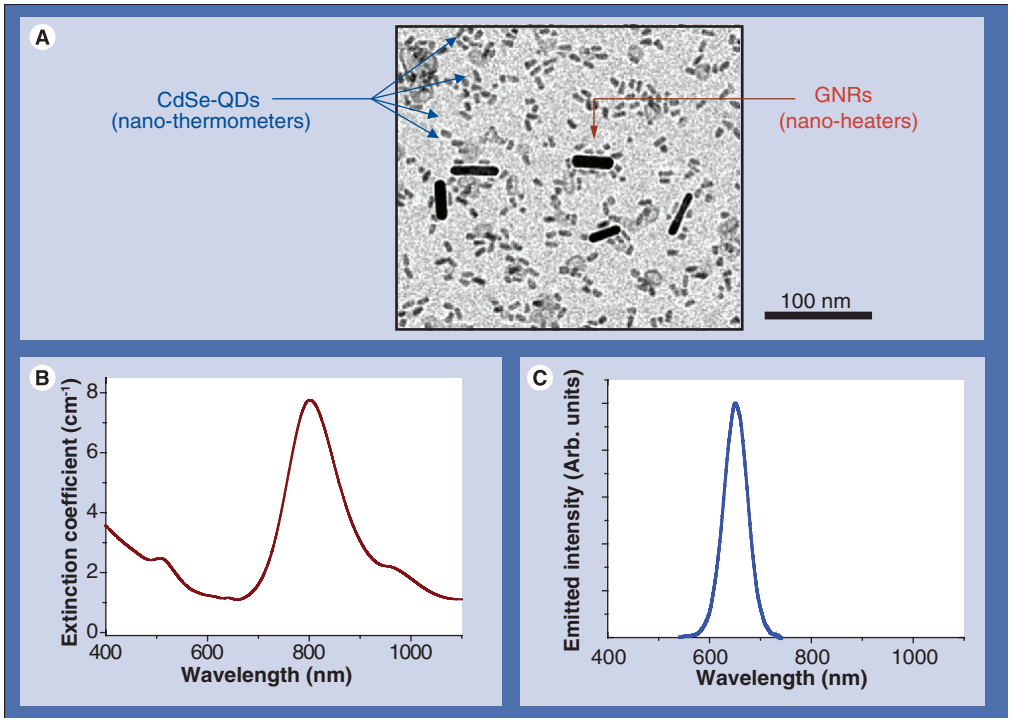

Figure 1. Transmission electron microscopy image and optical spectra of the (quantum dots + gold nanorods) solution. (A) Transmission electron microscopy image of a mixed solution of CdSe-QDs (acting as nanothermometers) and GNRs (used as nanoheaters) in which HeLa cells were incubated. **(B)** Room temperature extinction coefficient of the QDs:GNRs:phosphate-buffered saline solution. Note the strong optical extinction at 808 nm due to the longitudinal surface plasmon resonance of GNRs. **(C)** Room temperature emission spectrum of the QDs:GNRs:phosphate-buffered saline solution when excited at 488 nm. Note that it resembles the characteristic emission band of CdSe-QDs.
GNR: Gold nanorod; QD: Quantum dot.

solution under 488 nm laser excitation; only the emission band centered at 650 nm of CdSe-QDs is observed. Similar results were obtained when optical excitation was performed with near-infrared femtosecond laser pulses (i.e., through multiphoton excitation). The emission peak position of this band is highly temperature-sensitive (at a rate of 0.16 nm/°C), allowing for fluorescence nanothermometry as already described elsewhere [28].

At this point, it should be mentioned that prior to developing experiments in living cells, we have investigated the toxicity of both GNRs and CdSe-QDs in HeLa cancer cells. This is of special relevance, as previous works stated that, under certain conditions, deterioration of the CdSe lattice could lead to large levels of cytotoxicity [33]. Nevertheless, we have not found any evidence of enhanced cytotoxicity of HeLa cells incubated (for up to 4 h) with solutions containing GNRs and CdSe-QDs at the concentration levels used in this work. Indeed, this is in agreement with previous works that reported no significant toxicity for *in vitro* labeling of immortalized cell lines [34–36].

To investigate the simultaneous incorporation of NHs and NTs inside living cells, we used HeLa cells. These cells are an immortal cell line derived from a human cervical cancer, with an epithelial phenotype. They can divide an unlimited number of times *in vitro* with minimal cell survival conditions, and so they are widely used for cancer research [37]. Furthermore, HeLa cells present an additional advantage for our experiments. They derive from a type of cancer (uterine cervix) that is completely accessible to external laser sources, so that they constitute a realistic scenario to test the possibility of achieving laser-induced controlled hyperthermia. HeLa cells were incubated with the QDs:GNRs:PBS solution for 2 h at 37°C. After incubation, the successful internalization of the QDs and GNRs inside HeLa cells was studied by two-photon excited fluorescence microscopy using a fast multiphoton microscope (Zeiss LSM510 microscope). Figure 2 shows the optical transmission image (Figure 2A), the fluorescence image (Figure 2B), and the overlay images (Figure 2C) of a group of HeLa cancer cells incubated with the QDs:GNRs:PBS solution. Excitation and collection wavelengths were 800 and 650 nm,

respectively. These images unequivocally demonstrate the incorporation of the CdSe-QDs (predominant luminescent NPs) inside HeLa cancer cells. At this point it is important to remark that the CdSe-QDs solution concentration used in this work (4.8×10^{13} CdSe-QDs per cm^3) was found to be optimum, as it leads to a non-noisy intracellular emission spectrum, from which the temperature can be accurately determined. Lower CdSe-QDs concentrations reduced the intracellular signal-to-noise ratio that causes deterioration in the thermal sensitivity. On the other hand, the use of more concentrated solutions leads to the appearance of CdSe-QDs clusters and to a non-complete cell internalization of the CdSe-QDs. The intracellular emission spectrum was found to resemble that of CdSe-QDs (see Figure 1C) – that is, no fluorescence signature of intracellular GNRs was observed. As a consequence, the incorporation of GNRs was checked by examining the same HeLa cancer cells as incubated with the QDs:GNRs:PBS solution with a TEM microscope. Figure 2D shows a detail of a TEM image of a HeLa cell in which the cell's membrane can be clearly observed (as indicated in the image). Given the heterogeneity of the intracellular space, together with the small size of CdSe-QDs (see Figure 1A), CdSe-QDs are not

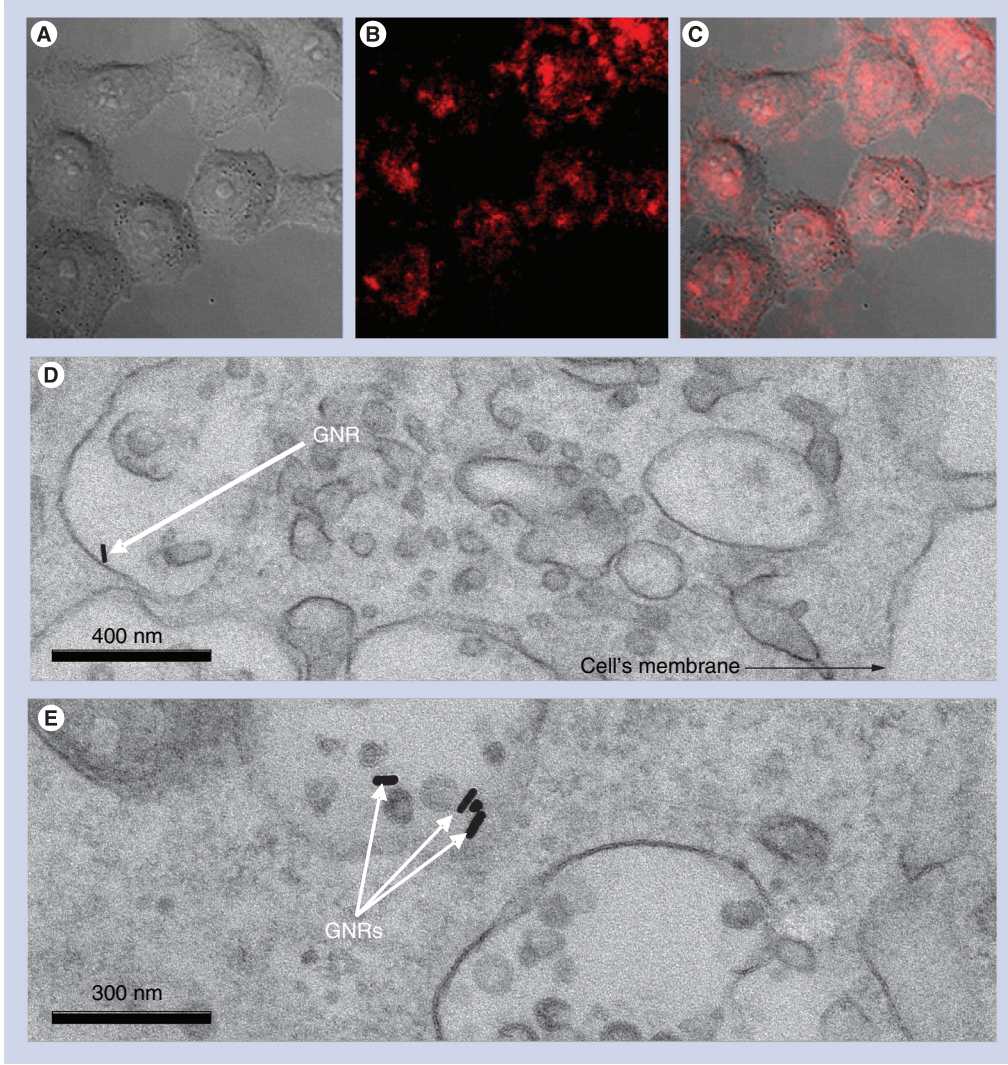

Figure 2. Incorporation of the solution nanoparticles into HeLa cells. (A) Optical transmission image, **(B)** fluorescence image and **(C)** the overlay image, of a group of HeLa cancer cells incubated at 37°C with the quantum dots:GNRs:phosphate-buffered saline solution. **(D)** Detail of a transmission electron microscopy image corresponding to a HeLa cancer cell incubated at 37°C with the quantum dots:GNRs:phosphate-buffered saline solution. The position of the cell membrane is indicated. The white arrow reveals the presence of a GNR inside a vesicle. This image evidences the intracellular incorporation of GNR. **(E)** Transmission electron microscopy image of an intracellular vesicle containing several GNRs.
GNR: Gold nanorod.

clearly seen. However, the presence of GNRs inside the cell was evidenced. Figure 2D shows the presence of a GNR (indicated by a white arrow) within a vesicle. This fact confirms the intracellular incorporation of GNRs by endocytosis. We have also found that the density of GNRs inside the vesicles of the HeLa cells is heterogeneous. In any case, the multiphoton microscope and TEM images included in Figure 2 confirm the simultaneous intracellular incorporation of both NTs and NHs inside HeLa cancer cells.

Both the multiphoton and TEM images of HeLa cells after incubation in the mixed solution have also been used to make a first estimation (first-order approximation) of the actual number of CdSe-QDs and GNRs internalized in the HeLa cells. For the estimation of the CdSe-QDs incorporated into cells, we made a rough approximation that provides an idea of the minimum number of dots inside each HeLa cell. We assigned each bright pixel in the multiphoton microscope images to a single CdSe-QD. Thus, the number of bright pixels inside the cell gives us a value of the minimum number of intracellular QDs. We have estimated that each cell contains, on average, at least 5000 CdSe-QDs. For the estimation of the number of GNRs incorporated into cells we have used different TEM images taken on different single cells. On average, we have found that the number of GNRs per cell is close to 200. Of course, these are only a first-order estimation, and more accurate determination of the number of cell-internalized NPs would require the performance of future specific experiments.

Once the successful incubation of HeLa cancer cells with both NTs and NHs was achieved, controlled hyperthermia experiments were conducted in a home-made double-beam confocal fluorescence microscope. HeLa cells were placed in a temperature-stabilized microscope slide. This slide was placed at the focal plane of two microscope objectives that focused two counter-propagating laser beams at the same point inside a single HeLa cell. One objective (60X, 0.65 NA) was used to focus an unpolarized diode laser beam down to a spot of 2 µm in diameter. This laser, tuned to the plasmon resonance wavelength of our GNRs (808 nm, see Figure 1), acts as the heating laser radiation, as schematically indicated in Figure 3A. The second objective (100X, 0.8 NA) was used to focus a 488 nm laser beam down to a spot of 1 µm, which was spatially overlapped with the 808 nm spot inside a HeLa cancer cell. The 488 nm radiation was used to provide optical excitation of the CdSe-QDs (QD-excitation beam in Figure 3A & B). The subsequently generated QDs

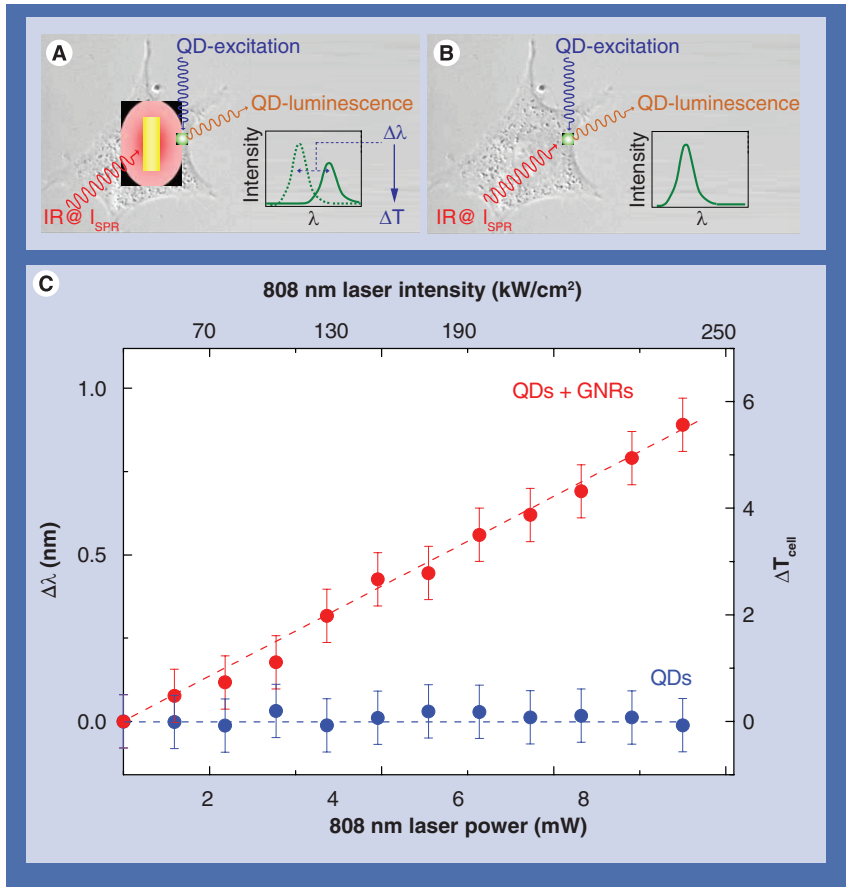

Figure 3. Temperature changes induced by gold nanorods. (A) Schematic representation of GNR-assisted intracellular heating and CdSe-QDs-mediated thermal reading. Note that both heating and thermal reading processes are laser activated. **(B)** Schematic representation of the same effect but in the absence of GNRs. Note that in this case no intracellular heating is expected. **(C)** Intracellular temperature increment (ΔT_{cell}) as a function of the heating laser power/intensity (808-nm laser power/intensity) induced in a single HeLa cancer cell in the presence/absence of GNRs (nanoheaters). Thermal reading has been obtained from the experimentally observed temperature-induced spectral shifts ($\Delta\lambda$) of the CdSe-QDs fluorescence band (displayed in the left axis).
GNR: Gold nanorod; QD: Quantum dot.

emission was collected by the same objective and, after passing several filters and apertures, analyzed with a high-resolution spectrometer. The emission spectra of CdSe-QDs were then carefully analyzed using a previously calibrated thermometric scale (not shown for the sake of brevity) based on the article by Maestro *et al.* [28], which provides the intracellular temperature as determined from the emission peak wavelength. Finally, an optical transmission microscope was used to monitor cell morphology at each stage of the experiment. The time period for all the experiments described in this work (including optical imaging of cells, as well as intracellular temperature determination) was set to 2 min (measured from the instant at which each 808 nm laser power was set). Note that the heating processes under investigation in this paper are produced in a volume in the

order of a few mm^3, so that thermalization times are not expected to be longer than a few seconds [38]. Therefore, the time interval between measurements used all along this work ensures a complete thermalization of the system.

Results & discussion

The ability of the above-described experimental set-up for real-time controlled hyperthermia is demonstrated in Figure 3C. In this figure, we show the intracellular temperature (as obtained from the analysis of the CdSe-QD luminescence) as a function of the 808 nm laser power. As expected, a linear relation between heating laser power and intracellular temperature is evidenced. Note that even for relatively low pump powers (7.5 mW, corresponding to a laser intensity close to 240 kW/cm^2), the intracellular temperature has been increased by almost 6°C. Such amount of heating is, therefore, capable of driving a cell initially at 37°C (human body temperature) up to the cytotoxic range (42–45°C) [39]. In order to unequivocally relate this laser-induced heating to the presence of GNRs (i.e., to the excitation of the plasmon resonance), the same experiments were performed on HeLa cancer cells but incubated with a solution containing only CdSe-QDs (in absence of GNRs), as schematically described in Figure 3B. Data obtained in this experiment are also included in Figure 3C. It is clear that, without the interplay of the surface plasmon oscillations, the 808 nm laser radiation does not cause any intracellular heating at all. Therefore, the only heating source inside cells must be from the GNRs that have been incorporated. In addition, we conclude that other possible 808 nm laser-induced absorption mechanisms (including water and cellular membrane absorption) are negligible, at least for the laser pump powers and focused conditions used all along this work. At this point, it has to be mentioned that the magnitude of this intracellular heating was found to depend on the concentration of GNRs. The use of a GNR concentration (in the order to 10^8 cm^{-3}) lower than that of our GNRs:QDs:PBS solution (5×10^9 cm^{-3}) leads to a negligible heating effect for the laser powers (laser intensities) available in our experimental conditions. On the other hand, incubation with larger GNR concentrations (in the order of 10^{10} cm^{-3}) leads to the appearance of GNR clusters and, hence, to nonreproducible results. Thus we estimate that the GNRs concentration used in this work can be considered close to the optimum one, at least for our experimental conditions. Finally, it should also be noted that further optimization of the laser-induced GNR-based hyperthermia treatment can be reached by an adequate design of laser polarization, as has already been stated by prior works [21,40]. In our experimental conditions, such a design is not possible due to the de-polarized nature of our 808 nm laser source. Nevertheless, future works will focus on this issue.

As mentioned above, the plasmonic-mediated laser-induced intracellular heating can be as large as 6°C and, in principle, this temperature increment is expected to have a strong effect on the morphology of the cells, since it is driven up to cytotoxic levels [39]. In order to corroborate this effect, we studied cellular morphological changes induced by the 808 nm heating laser in HeLa cancer cells incubated with QDs:GNRs:PBS, compared with HeLa cells incubated only with QDs:PBS. The corresponding optical transmission images are shown in Figure 4. We confirmed that even with relatively low laser powers (4 mW, corresponding to laser intensities close to 130 kW/cm^2), the correlated temperature increase (3°C, as measured by the CdSe-QDs) produces drastic cell morphology changes, as evidenced by a remarkable cell blebbing affecting cell membranes (see Figure 4A). A further increase of heating laser power up to 7.5 mW (≈240 kW/cm^2) produces a temperature increase of approximately 6°C with respect to the nonirradiated bath, so that cell death is clearly observed, with disappearance of nuclei and organelles, probably owing to intracellular disorganization. Temperature-induced cellular changes have been previously described, and they include protein denaturation, which leads to alterations in multimolecular structures like cytoskeleton and membranes, and changes in enzyme complexes for DNA synthesis and repair [39]. Given the short periods of time HeLa cells are exposed to additional heat (2 mins) during our experiments, the main mechanism for cell death as a consequence of hyperthermia treatment is most likely by necrosis owing to these molecular and structural effects. Apoptotic cell death is not feasible, since this process involves active gene transcription of proteins involved in DNA and protein damage (mainly caspases, proteases and nucleases), which requires longer periods of time [41]. The hyperthermia effects observed in our experiments are unequivocally related to the heat delivered by the GNRs. Consequently, as expected, no morphological changes of the cells are observed (see Figure 4B) when the 808 nm heating laser irradiates HeLa cells solely incubated with CdSe NTs.

Finally, it should be noted from Figure 4 that, although the 808 nm heating beam was focused

inside a single/individual cell (marked by an arrow in Figure 4), the thermal-induced morphological changes are induced not only on this cell, but also on the surrounding ones. We attributed this result to temperature diffusion effects. It is known that temperature distributions of a specimen locally heated by a tightly focused laser beam depends on several parameters, such as pulse duration, laser repetition rate, laser intensity, beam size and chamber geometries [40,42]. In our case we are dealing with 'continuous wave' lasers, so that the situation becomes less complicated. Mao *et al.* proposed (and verified) a simple model to describe thermal distributions in micro-chambers filled by a liquid that is locally heated by a tightly focused laser beam [43]. According to this model, and taking into account our experimental conditions (300 µm chamber height and heating spot size of 2 µm), the laser-induced heating is far from being spatially restricted to the laser focus. Indeed, it is expected that the laser-induced temperature change will spread over tens of microns around the laser focus. Indeed, this is in agreement with previously published experimental data on the study of localized laser-induced heating processes in liquids [43,44]. This is also in agreement with the recently published work by Donner *et al.*, who reported on remarkable cell heating by a tightly focused laser beam located 50 µm away from the cell under study [45]. As a consequence, although we are focusing our laser within a specific single cell, the steady-state temperature increment spreads over tens of microns around this cell. Indeed, this explains why temperature-induced morphological changes are also induced in the cells located in the surroundings of the laser focus.

Nevertheless, this temperature diffusion around the laser focus has been experimentally verified by additional measurements. Figure 5 shows the temperature spatial distribution measured in a QDs:GNR:PBS suspension within a 400 µm height micro-chamber when it is excited by a tightly focused 808 nm laser beam (similar experimental conditions as those adopted for our laser-induced hyperthermia experiments related to Figures 3 & 4). For the acquisition of this thermal image the experimental set-up had to be modified so that it was possible to scan the 488 nm excitation (reading) laser spot in the surroundings of the 808 nm laser heating focus. As can be observed, the laser-induced temperature increment spreads out over tens of microns in the surroundings of the 800 nm laser spot. These experimental data verify that in our photo-thermal treatments, and due to the thermal diffusivity of the medium, laser-induced heating is not only produced at the treated cell, but also in the surrounding cells. Since the 488-nm excitation beam is spatially overlapping with the 808 nm heating spot, the temperature increments reported in Figure 3 correspond to the maximum temperature achieved (i.e., to the temperature at focus).

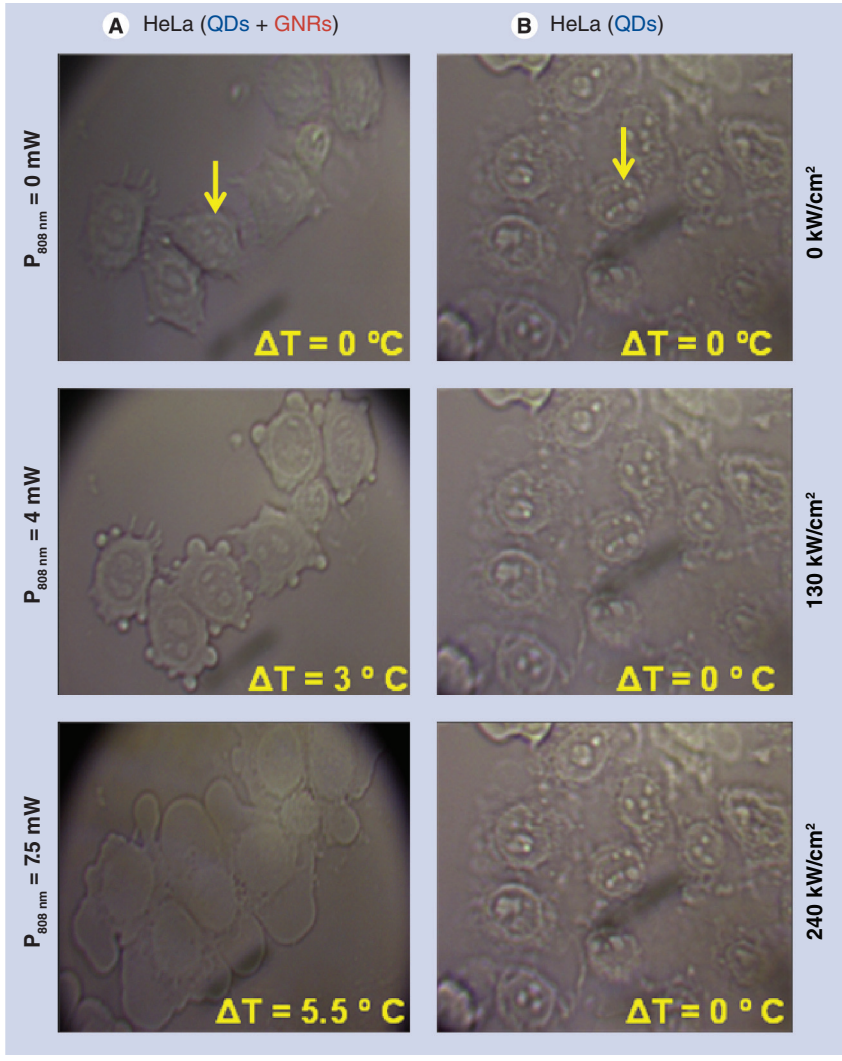

Figure 4. Photothermal effect of quantum dots:gold nanorods:phosphate-buffered saline solution on the morphology of HeLa cells. (A) Optical transmission images of HeLa cancer cells incubated with a solution containing both nanoheaters (GNRs) and nanothermometers (CdSe-QDs) for different 808 nm radiation powers/intensities. The intracellular temperature increment caused in each case is indicated. Note the presence of cell blebbing at intermediate 808 nm laser powers, indicating initiation of cell death processes. Further increment of the 808 nm laser power (heating power) causes massive cell death. Arrows indicate the particular cell within which the 808 nm laser beam is tightly focused. **(B)** Optical transmission images of HeLa cancer cells incubated with a solution containing only nanothermometers (CdSe-QDs) for different 808 nm radiation intensities. In the absence of GNRs, no intracellular laser-induced heating is registered.
GNR: Gold nanorod; QD: Quantum dot.

Conclusion

In summary, we have obtained experimental evidence about the potential use of quantum

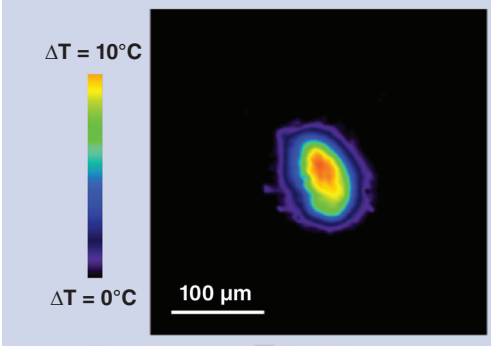

Figure 5. Thermal gradient. Temperature spatial distribution measured in a quantum dots:gold nanorods:phosphate-buffered saline solution suspension within a 400 μm height micro-chamber when it is excited by a tightly focused 808 nm laser beam (similar experimental conditions as those adopted during the laser-induced hyperthermia experiments of Figures 3 & 4). The 808 nm laser power and intensity was 10 mW and 320 kW·cm^{-2}, respectively. Note that the laser-induced temperature increment spreads out over tens of microns in the surroundings of the 800 nm laser spot.
For color images see online at www.futuremedicine.com/doi/10.2217/nnm.12.122.

dot fluorescence thermometry for real-time intracellular temperature read-out during plasmonic-mediated laser-induced hyperthermia of cultured cancer cells. This precise temperature read-out provides the possibility of settling operation limits for laser-induced hyperthermia processes, avoiding the creation of irreversible thermal damage in surrounding healthy cells and tissues, which is of crucial importance in real clinical management of patients.

Results here included constitute a new step towards controlled single-cell hyperthermia, essential for the early treatment, not only of cancer, but of other human pathologies in which undesirable cell proliferation exists, such as autoimmune disorders, diabetic retinopathy, keloid formation or acute rejection of transplanted organs. Moreover, from the perspective of *in vivo* applications of the methodology here presented, the fact that both GNRs and fluorescent NTs can be both excited with NIR radiation lying in the biological window (700–900 nm) makes them very promising for high tissue penetration and so for animal imaging and treatment. Thus, the future medical application of the methodology here demonstrated appears to be very promising.

Future perspective

Authors are convinced that controlled laser-induced hyperthermia will be fully addressed in the forthcoming years by taking advantage of the combination of NHs and NTs. This would be easy by using a similar approach to that described in this work. The critical point will be the actual penetration depth of the controlled hyperthermia treatments. The use of the GNRs and QDs working in the 800–900 nm spectral range will ensure penetration lengths of a few millimeters. Extending these penetration lengths up to the range of centimeters would require the use of other spectral windows (like the so-called 'second biological window' [1000–1300 nm]). Nevertheless, all these treatments would be based on 'the proof of concept' shown in this paper.

Financial & competing interests disclosure

This work was supported by the Universidad Autónoma de Madrid and Comunidad Autónoma de Madrid (Projects CCG087-UAM/MAT-4434 and S2009/MAT- 1756), by the Spanish Ministerio de Educación y Ciencia (MAT2010-16161 and MAT2010-21270-C04-02), Malta Consolider-Ingenio 2010 (CSD2007-0045), FPI grant by Agencia Canaria de Investigación del Gobierno de Canarias and by the Caja Madrid Foundation. The authors have no other relevant affiliations or financial involvement with any organization or entity with a financial interest in or financial conflict with the subject matter or materials discussed in the manuscript apart from those disclosed.

No writing assistance was utilized in the production of this manuscript.

Ethical conduct of research

The authors state that they have obtained appropriate institutional review board approval or have followed the principles outlined in the Declaration of Helsinki for all human or animal experimental investigations. In addition, for investigations involving human subjects, informed consent has been obtained from the participants involved.

Executive summary

- Real-time laser-induced controlled hyperthermia implies the simultaneous use of nanoheaters (NHs) and nanothermometers (NTs). Nowadays, the two most promising NHs and NTs are the gold nanorods and semiconductor quantum dots, respectively.
- We have been able to simultaneously incorporate NHs and NTs in cancer cells. We have been also able to build up a double beam confocal microscope that allows cell heating and temperature reading in a simultaneous way.
- We provide evidence of controlled laser-induced hyperthermia at the cellular level. Temperature reading was obtained during hyperthermia treatment allowing for an unequivocal identification of the laser-induced morphological changes taking place during treatment.

References

Papers of special note have been highlighted as:
▪ of interest

1 Zhang L, Gu FX, Chan JM, Wang AZ, Langer RS, Farokhzad OC. Nanoparticles in medicine. Therapeutic applications and developments. *Clin. Pharmacol. Ther.* 83(5), 761–769 (2008).

2 Wagner V, Dullaart A, Bock AK, Zweck A. The emerging nanomedicine landscape. *Nat. Biotechnol.* 24(10), 1211–1217 (2006).

3 Bruchez M, Moronne M, Gin P, Weiss S, Alivisatos AP. Semiconductor nanocrystals as fluorescent biological labels. *Science* 281(5385), 2013–2016 (1998).

▪ **Quantum dots are regarded as one of the most promising fluorescent biological labels due to a unique combination of properties.**

4 Wang X, Yang L, Chen Z, Shin DM. Application of nanotechnology in cancer therapy and imaging. *CA Cancer J. Clin.* 58(2), 97–110 (2008).

5 Wang F, Banerjee D, Liu YS, Chen XY, Liu XG. Upconversion nanoparticles in biological labeling, imaging, and therapy. *Analyst* 135(8), 1839–1854 (2010).

6 Vetrone F, Naccache R, De La Fuente AJ *et al.* Intracellular imaging of HeLa cells by Am. J. Physiol. Heart C-functionalized $NaYF_4$:Er^{3+}, Yb^{3+} upconverting nanoparticles. *Nanoscale* 2(4), 495–498 (2010).

7 Gao Xh, Cui YY, Levenson RM, Chung LWK, Nie SM. *In vivo* cancer targeting and imaging with semiconductor quantum dots. *Nat. Biotech.* 22(8), 969–976 (2004).

8 Misgeld T, Kerschensteiner M. *In vivo* imaging of the diseased nervous system. *Nat. Rev. Neurosci.* 7(6), 449–463 (2006).

9 Ntziachristos V, Ripoll J, Wang LHV, Weissleder R. Looking and listening to light: the evolution of whole-body photonic imaging. *Nat. Biotech.* 23(3), 313–320 (2005).

10 Medintz IL, Uyeda HT, Goldman ER, Mattoussi H. Quantum-dot bioconjugates for imaging, labelling and sensing. *Nat. Mat.* 4(6), 435–446 (2005).

11 Gao XH, Chan WCW, Nie SM. Quantum-dot nanocrystals for ultrasensitive biological labeling and multicolor optical encoding. *J. Biomed. Opt.* 7(4), 532–537 (2002).

12 Brannon-Peppas L, Blanchette JO. Nanoparticle and targeted systems for cancer therapy. *Adv. Drug Deliv. Rev.* 56(11), 1649–1659 (2004).

13 Huff TB, Tong L, Zhao Y, Hansen MN, Cheng JX, Wei A. Hyperthermic effects of gold nanorods on tumor cells. *Nanomedicine* 2(1), 125–132 (2007).

▪ **Gold nanorods constitute a new generation of nanothermometers with real application in cancer treatment.**

14 Dickerson EB, Dreaden EC, Huang XH *et al.* Gold nanorod assisted near-infrared plasmonic photothermal therapy (PPTT) of squamous cell carcinoma in mice. *Cancer Lett.* 269(1), 57–66 (2008).

15 Huang HC, Rege K, Heys JJ. Spatiotemporal temperature distribution and cancer cell death in response to extracellular hyperthermia induced by gold nanorods. *ACS Nano* 4(5), 2892–2900 (2010).

16 Loo C, Lin A, Hirsch L *et al.* Nanoshell-enabled photonics-based imaging and therapy of cancer. *Technol. Cancer Res. Treat.* 3(1), 33–40 (2004).

17 Chen J, Wang D, Xi J *et al.* Immuno gold nanocages with tailored optical properties for targeted photothermal destruction of cancer cells. *Nano Lett.* 7(5), 1318–1322 (2007).

18 Tuchina ES, Tuchin VV, Khlebtsov BN, Khlebtsov NG. Phototoxic effect of conjugates of plasmon-resonance nanoparticles with indocyanine green dye on staphylococcus aureus induced by IR laser radiation. *Quantum Electron* 41(4), 354–359 (2011).

19 Maestro LM, Haro-Gonzalez P, Coello JG, Jaque D. Absorption efficiency of gold nanorods determined by quantum dot fluorescence thermometry. *Appl. Phys. Lett.* 100(20), 201110 (2012).

▪ **Gold nanorods could provide laser-to-heat conversion efficiencies close to 100%.**

20 Terentyuk GS, Maslyakova GN, Suleymanova LV *et al.* Laser-induced tissue hyperthermia mediated by gold nanoparticles: toward cancer phototherapy. *J. Biomed. Opt.* 14(2), 021016 (2009).

21 Kang H, Jia BH, Li JL, Morrish D, Gu M. Enhanced photothermal therapy assisted with gold nanorods using a radially polarized beam. *Appl. Phys. Lett.* 96(6), 063702 (2010).

22 Jo Jo W, Freedman K, Yi DK *et al.* Photon to thermal response of a single patterned gold nanorod cluster under near-infrared laser irradiation. *Biofabrication* 3(1), 015002 (2011).

23 Arthur RM, Straube WL, Trobaugh JW, Moros EG. Non-invasive estimation of hyperthermia temperatures with ultrasound. *Int. J. Hyperther.* 21(6), 589–600 (2005).

24 Paulsen KD, Moskowitz MJ, Ryan TP, Mitchell SE, Hoopes PJ. Initial *in vivo* experience with EIT as a thermal estimator during hyperthermia. *Int. J. Hyperther.* 12(5), 573–591 (1996).

25 Meaney PM, Paulsen KD, Hartov A, Crane RK. Microwave imaging for tissue assessment: Initial evaluation in multitarget tissue-equivalent phantoms. *IEEE Trans. Biomed. Eng.* 43(9), 878–890 (1996).

26 Hynynen K, Chung A, Fjield T *et al.* Feasibility of using ultrasound phased arrays for MRI monitored non-invasive surgery. *IEEE Trans. Ultras. Ferroelectr. Freq. Control* 43(6), 1043–1053 (1996).

27 Carter DL, Macfall JR, Clegg ST *et al.* Magnetic resonance thermometry during hyperthermia for human high-grade sarcoma. *Int. J. Radiat. Oncol.* 40(4), 815–822 (1998).

28 Maestro LM, RodrÍguez EM, RodrÍguez FM *et al.* CdSe quantum dots for two-photon fluorescence thermal imaging. *Nano Lett.* 10(12), 5109–5115 (2010).

▪ **CdSe-quantum dots can behave as high-resolution biocompatible nanothermometers.**

29 Yang JM, Yang H, Lin L. Quantum dot nano thermometers reveal heterogeneous local thermogenesis in living cells. *ACS Nano* 5(6), 5067–5071 (2011).

▪ **Quantum dots provide an intracellular thermal sensitivity good enough to monitor small intracelullar events that are accompanied by slight temperature variations.**

30 Maestro LM, Jacinto C, Silva UR *et al.* CdTe quantum dots as nano-thermometers: towards highly sensitive thermal imaging. *Small* 7(13), 1774–1778 (2011).

31 Choi HS, Liu W, Liu F *et al.* Design considerations for tumour-targeted nanoparticles. *Nat. Nano.* 5(1), 42–47 (2010).

32 Maestro LM, Rodriguez EM, Vetrone F *et al.* Nanoparticles for highly efficient multiphoton fluorescence bioimaging. *Opt. Express* 18(23), 23544–23553 (2010).

33 Derfus AM, Chan WCW, Bhatia SN. Probing the cytotoxicity of semiconductor quantum dots. *Nano Lett.* 4(1), 11–18 (2004).

34 Parak WJ, Boudreau R, Le Gros M *et al.* Cell motility and metastatic potential studies based on quantum dot imaging of phagokinetic tracks. *Adv. Mater.* 14(12), 882–885 (2002).

35 Jaiswal JK, Mattoussi H, Mauro JM, Simon SM. Long-term multiple color imaging of live cells using quantum dot bioconjugates. *Nat. Biotech.* 21(1), 47–51 (2003).

36 Wu X, Liu H, Liu J *et al.* Corrigendum: Immunofluorescent labeling of cancer marker Her2 and other cellular targets with semiconductor quantum dots. *Nat. Biotech.* 21(4), 452–452 (2003).

37 Masters JR. HeLa cells 50 years on: the good, the bad and the ugly. *Nat. Rev. Cancer* 2(4), 315–319 (2002).

- **HeLa cells provide a universally recognized scenario for cancer studies at the cellular level.**

38 Richardson HH, Carlson MT, Tandler PJ, Hernandez P, Govorov AO. Experimental and theoretical studies of light-to-heat conversion and collective heating effects in metal nanoparticle solutions. *Nano Lett.* 9(3), 1139–1146 (2009).

39 Roti Roti JL. Cellular responses to hyperthermia (40–46 degrees C): cell killing and molecular events. *Int. J. Hyperther.* 24(1), 3–15 (2008).

40 Avetisyan YA, Yakunin AN, Tuchin VV. Novel thermal effect at nanoshell heating by pulsed laser irradiation: hoop-shaped hot zone formation. *J. Biophotonics* doi:10.1002/jbio.201100074 (2011) (Epub ahead of print).

41 Vorotnikova E, Ivkov R, Foreman A, Tries M, Braunhut SJ. The magnitude and time-dependence of the apoptotic response of normal and malignant cells subjected to ionizing radiation versus hyperthermia. *Int. J. Radiat. Biol.* 82(8), 549–559 (2006).

42 Avetisyan YA, Yakunin AN, Tuchin VV. Thermal energy transfer by plasmon-resonant composite nanoparticles at pulse laser irradiation. *Appl. Opt.* 51(10), C88–C94 (2012).

43 Mao HB, Arias-Gonzalez JR, Smith SB, Tinoco I, Bustamante C. Temperature control methods in a laser tweezers system. *Biophys. J.* 89(2), 1308–1316 (2005).

44 Celliers PM, Conia J. Measurement of localized heating in the focus of an optical trap. *Appl. Opt.* 39(19), 3396–3407 (2000).

45 Donner JS, Thompson SA, Kreuzer MP, Baffou G, Quidant R. Mapping intracellular temperature using green fluorescent protein. *Nano Lett.* 12(4), 2107–2111 (2012).